

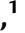

















Eukaryote-specific assembly factor DEAP2 mediates an early step of photosystem II assembly in Arabidopsis

Jakob-Maximilian Keller ¹, Maureen Julia Frieboes ¹, Ludwig Jödecke ¹, Sandrine Kappel ¹, Natalia Wulff ¹, Tobias Rindfleisch ², Omar Sandoval-Ibanez ¹, Ines Gerlach ¹, Wolfram Thiele ¹, Ralph Bock ¹, Jürgen Eirich ³, Iris Finkemeier ³, Danja Schünemann ⁴, Reimo Zoschke ¹, Mark Aurel Schöttler ¹ and Ute Armbruster ^{1,5,6,*}

- 1 Max Planck Institute of Molecular Plant Physiology, Potsdam Science Park, 14476 Potsdam, Germany
- 2 Computational Biology Unit, Department of Chemistry, University of Bergen, 5008 Bergen, Norway
- 3 Plant Physiology, Institute of Plant Biology and Biotechnology, University of Münster, 48143 Münster, Germany
- 4 Molecular Biology of Plant Organelles, Ruhr University Bochum, 44780 Bochum, Germany
- 5 Institute of Molecular Photosynthesis, Heinrich Heine University Düsseldorf, 40225 Düsseldorf, Germany
- 6 CEPLAS - Cluster of Excellence on Plant Sciences, Heinrich Heine University Düsseldorf, 40225 Düsseldorf, Germany

*Author for correspondence: ute.armbruster@hhu.de (U.A.)

The author responsible for distribution of materials integral to the findings presented in this article in accordance with the policy described in the Instructions for Authors (<https://academic.oup.com/plphys/pages/General-Instructions>) is Ute Armbruster (ute.armbruster@hhu.de).

Abstract

The initial step of oxygenic photosynthesis is the thermodynamically challenging extraction of electrons from water and the release of molecular oxygen. This light-driven process, which is the basis for most life on Earth, is catalyzed by photosystem II (PSII) within the thylakoid membrane of photosynthetic organisms. The biogenesis of PSII requires a controlled step-wise assembly process of which the early steps are considered to be highly conserved between plants and their cyanobacterial progenitors. This assembly process involves auxiliary proteins, which are likewise conserved. In the present work, we used *Arabidopsis thaliana* as a model to show that in plants, a eukaryote-exclusive assembly factor facilitates the early assembly step, during which the intrinsic antenna protein CP47 becomes associated with the PSII reaction center (RC) to form the RC47 intermediate. This factor, which we named DECREASED ELECTRON TRANSPORT AT PSII (DEAP2), works in concert with the conserved PHOTOSYNTHESIS AFFECTED MUTANT 68 (PAM68) assembly factor. The *deap2* and *pam68* mutants showed similar defects in PSII accumulation and assembly of the RC47 intermediate. The combined lack of both proteins resulted in a loss of functional PSII and the inability of plants to grow photoautotrophically on the soil. While overexpression of *DEAP2* partially rescued the *pam68* PSII accumulation phenotype, this effect was not reciprocal. *DEAP2* accumulated at 20-fold higher levels than *PAM68*, together suggesting that both proteins have distinct functions. In summary, our results uncover eukaryotic adjustments to the PSII assembly process, which involve the addition of *DEAP2* for the rapid progression from RC to RC47.

Introduction

Life on Earth is shaped by the production of molecular oxygen by photosynthetic organisms. Molecular oxygen is released during the initial step of photosynthesis, in which light energy is used to extract electrons from water. This thermodynamically demanding reaction is catalyzed by the

photosystem II (PSII) multiprotein complex. Under natural light conditions, plant PSII undergoes continuous damage, disassembly, and repair (Komenda et al. 2012; Nickelsen and Rengstl 2013; Lu 2016). A mechanistic understanding of PSII biogenesis and repair in plants is pivotal on multiple levels. Besides providing fundamental insight into plant's

Received May 12, 2023. Accepted July 06, 2023. Advance access publication August 9, 2023

© The Author(s) 2023. Published by Oxford University Press on behalf of American Society of Plant Biologists.

This is an Open Access article distributed under the terms of the Creative Commons Attribution License (<https://creativecommons.org/licenses/by/4.0/>), which permits unrestricted reuse, distribution, and reproduction in any medium, provided the original work is properly cited.

Open Access

bioenergetic blueprint, it can stipulate strategies to enhance crop yield by optimizing photosynthesis or support synthetic biology-based methods to harness light energy.

PSII constitutes a light-driven oxidoreductase localized in the photosynthetic thylakoid membrane, which oxidizes water at the lumen side and via a sequence of redox reactions reduces the membrane integral plastoquinone electron carrier at the stromal side. This life-defining molecular machine contains nuclear and plastid-encoded protein subunits and in the functional form of a plant supercomplex consists of a total of more than 500 components (Shen 2015; Wei et al. 2016). All these constituents have to be assembled in a concerted fashion to obtain a functional complex. Multiple cofactors, which either absorb light energy such as chlorophylls or are highly reactive such as hemes and the manganese cluster require integration simultaneously with the protein assembly process. Thus, a highly organized and step-wise assembly procedure is fundamental to avoid early damage of the nascent protein complex by the formation of highly reactive intermediates (Zagari et al. 2017; Shevela et al. 2019). This involves the function of molecular chaperones, which are referred to as PSII assembly factors.

In the early steps of PSII biogenesis, the core proteins are assembled to form the reaction center (RC) assembly intermediate. This intermediate consists of the subunits E and F (PsbE and F), together forming cytochrome b_{559} , the low molecular mass PsbI, as well as D1 and D2, which bind most redox-active cofactors of rapid electron transport within PSII (reviewed by Komenda et al. 2012; Nickelsen and Rengstl 2013; Lu 2016). Then, the addition of the intrinsic antenna CP47 and PsbH, PsbR, and PsbTc leads to the formation of the so-called RC47 assembly intermediate (Komenda et al. 2004; Rokka et al. 2005). Subsequently, the intrinsic antenna CP43, multiple small membrane-intrinsic subunits, and the extrinsic subunits PsbO, PsbP, and PsbQ, which stabilize the oxygen-evolving complex, are added to derive the PSII monomer. Ultimately, two PSII monomers form a PSII dimer and bind additional light-harvesting complexes to give rise to PSII supercomplexes (SC; Shevela et al. 2016).

The first assembly steps up to RC47 proceed in plant chloroplast in a very similar way as in cyanobacteria. Almost all known assembly factors involved in the formation of RC47 in plants have putative orthologs in cyanobacteria, further arguing for the evolutionary conservation of these early steps of the assembly process (Nickelsen and Rengstl 2013; Lu 2016). In *Arabidopsis* (*Arabidopsis thaliana*), RC assembly requires multiple essential factors that facilitate thylakoid membrane targeting, protein insertion and folding, as well as assembly. Mutants that lack these factors cannot form functional PSII and thus are unable to grow photoautotrophically (Meurer et al. 1998; Link et al. 2012; Lu 2016; Myouga et al. 2018; Li et al. 2019). Plants that lack LOW PSII ACCUMULATION1 (LPA1) can still assemble some functional PSII, but levels are strongly decreased, which leads to severely delayed growth compared with wild type (WT) on soil (Peng et al. 2006). LPA1 was shown to associate with nascent D1 to promote the formation of

the RC intermediate (Peng et al. 2006; Armbruster et al. 2010). For the next step in PSII assembly, which is the progression from RC to RC47, so far only one specific assembly factor has been described, which is the PHOTOSYNTHESIS AFFECTED MUTANT 68 (PAM68) protein (Armbruster et al. 2010). Plants lacking PAM68 display a slowing down of PSII assembly directly after the RC intermediate. This leads to a similar phenotype as in the *lpa1* mutant with low PSII accumulation and slow growth (Armbruster et al. 2010). The cyanobacterial ortholog of PAM68 from *Synechocystis* PCC 6803 was found to interact with ribosomes and promote CP47 synthesis, and it was suggested that PAM68 is involved in the cotranslational insertion of chlorophyll into CP47 (Bučinská et al. 2018). In *Arabidopsis*, however, no differences could be observed for the synthesis of CP47 between *pam68* mutants and WT (Armbruster et al. 2010), questioning whether this function of PAM68 is conserved between plants and cyanobacteria.

In the present study, we discovered a plant assembly factor for the early stages of PSII biogenesis not conserved in cyanobacteria and named it DECREASED ELECTRON TRANSPORT AT PSII (DEAP2). We demonstrate that DEAP2 acts in concert with the evolutionary conserved PAM68 to facilitate the progression of PSII assembly from the RC to the RC47 intermediate.

Results

Lack of DEAP2 affects plant growth, pigmentation, and PSII function

During an initial screen of *Arabidopsis* T-DNA insertion lines under fluctuating light conditions, we found that the mutants of the line SALK_048033 grew very slowly and had chlorotic leaves (Supplemental Fig. S1). When grown under low nonfluctuating light conditions, these mutants still showed a strong growth retardation and paler leaves. Salk_048033 carries a T-DNA insertion in the gene *At3g51510* (Fig. 1A). To confirm that *At3g51510* was the causal gene for the observed phenotype, two more mutants were generated via CRISPR-Cas gene editing. Under low-light conditions, all plants with lesions in *At3g51510* showed the same slow growth and pale leaf phenotype, which was complemented by the introduction of the *At3g51510* cDNA expressed from the 35S promoter into SALK_048033 (Fig. 1B, Supplemental Fig. S2A). All three independent *at3g51510* mutants showed a strong decrease in the maximum quantum efficiency of PSII in the dark-adapted state (Fv/Fm) and were thus termed *decreased electron flow at PSII* (*deap2*) with the two analyzed complemented lines being referred to as *cDEAP2-1* and *-2* (Fig. 1B). We confirmed the absence of DEAP2 protein in all three *deap2* lines by generating a specific antibody against the 18 most C-terminal amino acids of the protein (Supplemental Fig. S2B, C). While no protein was detected in the mutants, an upward shift of the signal was detected in the *cDEAP2* lines compared with the WT. The *cDEAP2* lines carry a Myc-tag at the C-terminal end of DEAP2, which adds 1.2 kDa to the protein. The growth, chlorophyll (Chl)

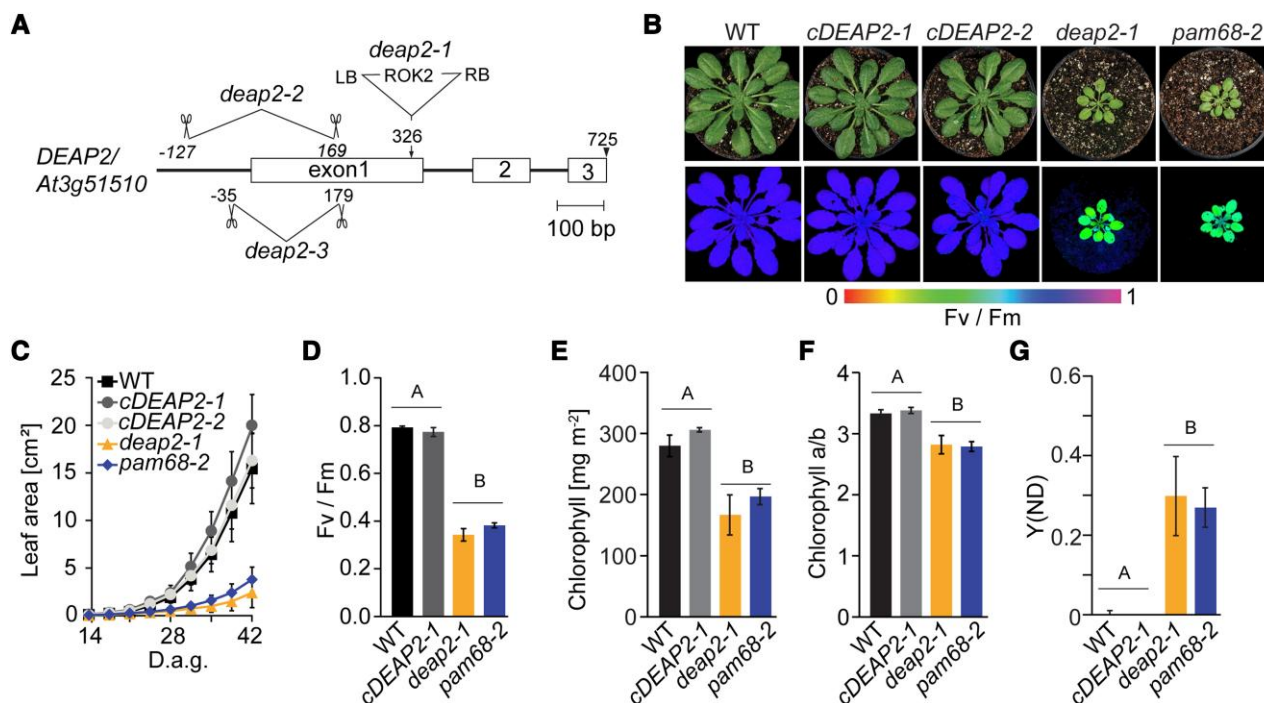


Figure 1. The *deap2* mutant shows a defect in growth, pigmentation, and PSII function comparable to the PSII assembly factor deficient *pam68*. **A)** Map of the gene locus *DEAP2/At3g51510*. Exons are displayed as white boxes, introns as black lines. Location of the T-DNA insertion in *deap2-1* (SALK_048033) and the deletions obtained by CRISPR/Cas, *deap2-2*, and *deap2-3* are shown. Deletions are indicated by scissors giving the cutting site relative to the start codon as determined by sequencing of genomic DNA from these lines (LB, left T-DNA border; RB, right T-DNA border). **B)** Pictures (top panel) and PSII maximum quantum yield (Fv/Fm) false color images taken with the Imaging-PAM (bottom panel) of 8-week-old Columbia-0 (wild type, WT), two independent complementation lines, *cDEAP2-1* and *cDEAP2-2*, *deap2-1* and *pam68-2* (top panel) grown at 50 $\mu\text{mol photons m}^{-2} \text{s}^{-1}$ with a 12/12 h light/dark cycle. Signal intensities for Fv/Fm are given by the false color scale below the panels. **C)** Increase in leaf area of the different genotypes measured from 14 to 42 days after germination (d.a.g.). Shown is the average of $n = 10 \pm \text{SD}$. **D to G)** Bar graphs of PSII maximum quantum yield (Fv/Fm) **D)**, chlorophyll content per leaf area **E)**, chlorophyll a/b ratio **F)**, and quantum yield of nonphotochemical energy dissipation due to donor side limitation of PSI (Y(ND)) at growth light intensity **G)**. Average is shown of $n = 5$ to $9 \pm \text{SD}$. The capital letters above the graphs denote the two significantly different groups ($P < 0.05$) as determined by one-way ANOVA and Holm-Sidak multiple comparison test.

content, and Fv/Fm phenotypes of *deap2* mutants were similar to that of the previously reported *pam68* mutant, which is defective in the assembly of the RC47 intermediate of PSII (Armbruster et al. 2010; Fig. 1C to F). The reduced Chl a/b ratio indicated a stronger loss of photosystem reaction centers (binding only Chl a) relative to antenna proteins (binding both Chl a and b) in the two mutants. By analyzing the PSI donor side limitation under growth light intensity, we found that it was severely increased to the same degree in *deap2* and *pam68* compared with WT and *cDEAP2*. This result showed that linear electron transport towards PSI was decreased, supporting that the activity of PSII was more negatively affected than PSI in both mutants (Fig. 1G).

DEAP2 is a eukaryote-specific thylakoid membrane protein found only in the green lineage

For localization, the C-terminus of DEAP2 was fused to yellow fluorescent protein (YFP), and the respective construct was transiently expressed in leaves of *Nicotiana benthamiana*.

This experiment revealed that DEAP2 colocalizes with Chl a fluorescence in the chloroplast (Fig. 2A). To further investigate the localization of DEAP2, we isolated intact chloroplasts from Arabidopsis WT rosettes and fractionated them into envelope and thylakoid membranes as well as soluble stroma. Immunoblot analysis using the specific DEAP2 antibody confirmed the exclusive localization of DEAP2 in the thylakoid membrane together with the Chl-binding light-harvesting protein Lhcb1 (Fig. 2B, lower panel). Treatment of WT thylakoids with chaotropic salts revealed that only little of the DEAP2 protein could be extracted, which is consistent with this protein constituting a thylakoid integral protein (Fig. 2C), thus supporting the prediction of two transmembrane helices (Fig. 2D).

A predicted chloroplast transit peptide (cTP) cleavage site around alanine (A) 59 of the precursor protein was supported by mass spectrometry (MS) analysis of enriched mature DEAP2 from the thylakoid membrane, which only detected peptides C-terminal of this site (Fig. 2D, Supplemental Tables S1 and S2). The molecular weight of

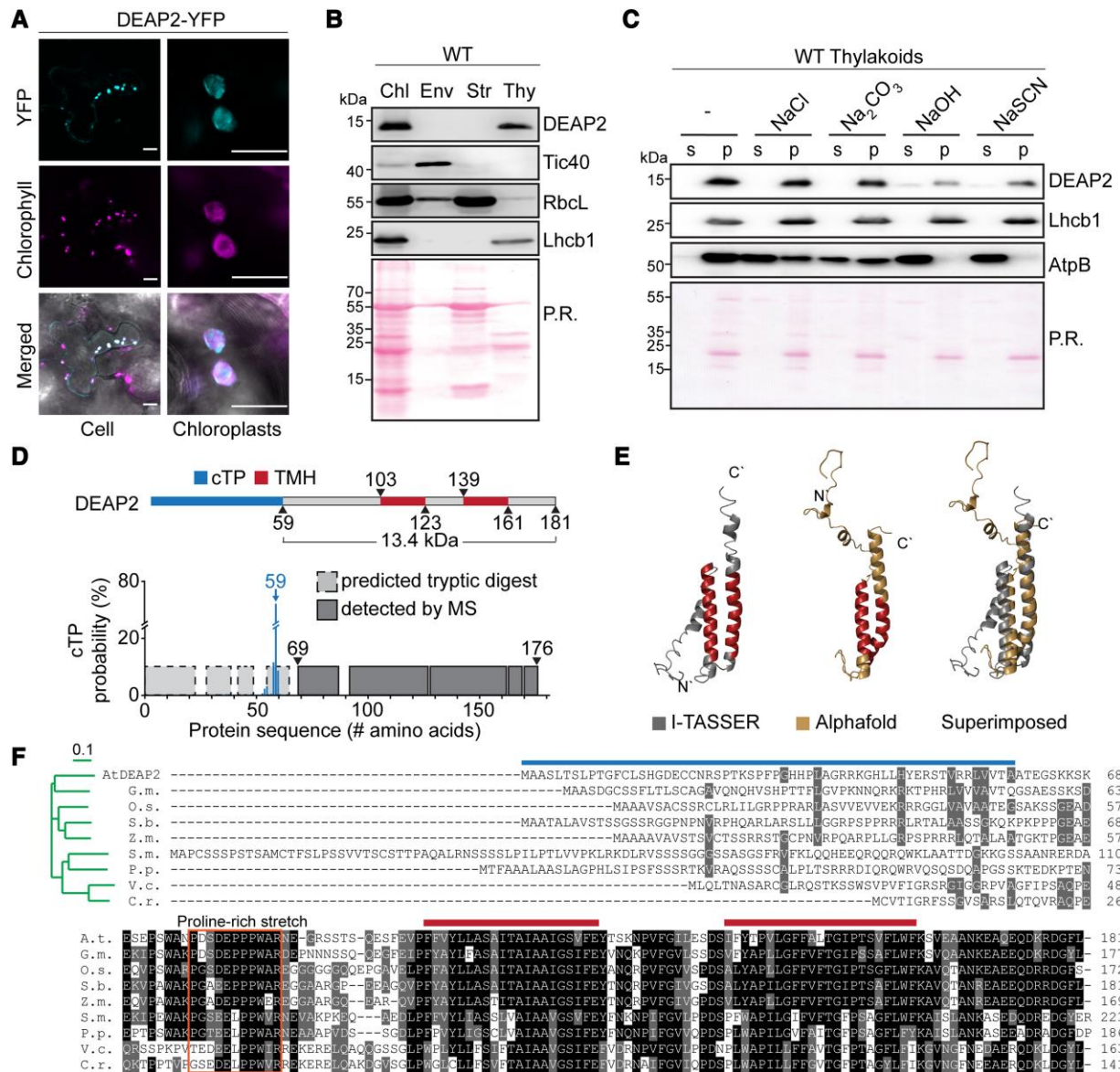


Figure 2. DEAP2 is a thylakoid integral protein conserved in the eukaryotic green lineage. **A)** Localization of DEAP2 fused to the yellow fluorescent protein (YFP) at its C-terminus in *Nicotiana benthamiana* by fluorescence microscopy. The individual signals of YFP (top panel), chlorophyll (middle panel) and a merged image (bottom) of a cell (left) and individual chloroplasts (right) are shown. Scale bar represents 25 μ m and 10 μ m on left and right, respectively. **B)** Immunoblots using the specific DEAP2 antibody show the protein localizes in the thylakoid membrane: proteins of whole chloroplasts (Chl), envelope (Env), stroma (Str) and thylakoids (Thy) from wild type (WT) were probed for DEAP2, Tic40 as a control for the envelope membrane, RbcL as a control for the stroma and Lhcb1 as a control for the thylakoid membrane. **C)** WT thylakoids were incubated either with buffer only (–) or added NaCl, Na₂CO₃, NaOH, or NaSCN and subsequently separated into pellet (p) and supernatant (s) fractions by centrifugation. Immunodetection was carried out on fraction using antibodies against DEAP2, Lhcb1 as a membrane integral control and AtpB as a membrane associated control. **B and C)** Ponceau staining (P.R.) of the membrane prior to immunodetection is shown. Numbers left of the immunoblots indicate molecular weight in kDa of protein standards. **D)** Protein model of DEAP2 with predicted chloroplast targeting peptide (cTP) and transmembrane helices (TMH). cTP cleavage site prediction by TargetP was supported by mass spectrometry (MS)-based detection of tryptic peptides from mature DEAP2 enriched from the thylakoid membrane of *cDEAP2-1* by using a Myc-trap. **E)** Protein structure of mature DEAP2 predicted by AlphaFold and I-TASSER and both structures superimposed. C' and N' mark the C- and N-terminus of the protein, respectively. **F)** Sequence alignment and phylogenetic reconstructions (green tree as calculated by the Neighbor-joining method of Clustal Omega with the scale bar reflecting the relative evolutionary distance between the species) of DEAP2 homologs of soybean [*Glycine max* (G.m.)], Rice [*Oryza sativa* (O.s.)], sorghum [*Sorghum bicolor* (S.b.)], corn [*Zea mays* (Z.m.)], the mosses *Sphagnum maghellanicum* (S.m.) and *Physcomitrium patens* (P.p.), and the green algae *Volvox carteri* (V.c.) and *Chlamydomonas reinhardtii* (C.r.). 50% to <100% sequence similarity is marked grey and 100% black. Lines above sequences indicate cTP and TMH as in (D). The box around a stretch of conserved amino acids N-terminal of the two TMHs indicates a conserved proline-rich domain.

the mature DEAP2 protein was predicted to be 13.4 kDa, consistent with the immunoblots, which showed that the WT and Myc-tagged DEAP2 proteins migrated just below or at the same height as the 15 kDa marker protein band, respectively (Fig. 2B). Protein structure predictions suggested both transmembrane helices (TMH) of the Arabidopsis DEAP2 to be connected via an unstructured region and to extend to the C-terminus as a helical structure (Fig. 2E). The DEAP2 protein is conserved in the green lineage of photosynthetic eukaryotes (Fig. 2F; Karpowicz et al. 2011). Besides a high conservation of the region encompassing the two TMHs and the C-terminus, the protein shows a conserved domain in the N-terminus of the mature protein, which is proline-rich with an increasing number of prolines during the evolution from algae to vascular plants.

Loss of DEAP2 has negative consequences specifically for the accumulation of PSII

To obtain further insight into the accumulation of thylakoid protein complexes in the *deap2* mutant, we performed immunoblot analyses on thylakoid membrane proteins of WT, *cDEAP2-1*, *deap2-1*, and *pam68-2* corresponding to the same amount of Chl, isolated from rosettes of low-light grown plants. By using a WT dilution series, we could show that all PSII subunits were decreased to ~40% of WT in both *deap2-1* and *pam68-2* (Fig. 3A). When comparing both mutants with WT for other thylakoid complexes, on the basis of equal Chl, strong increases were found for the Cyt *b₆f* and the NADPH-dehydrogenase (NDH) complexes as determined by PetA and NdhB antibodies, respectively, and a mild increase for LHClI as detected by the Lhcb1 antibody. The chloroplast ATP synthase and PSI as detected by AtpB and PsaA antibodies, respectively, showed mild decreases. In parallel, PSII, PSI, and Cyt *b₆f* complexes were quantified spectroscopically (Fig. 3B). The results from this analysis supported the quantification by immunoblot analysis. In all experiments, the *cDEAP2-1* line showed comparable results to WT. The apparent increases in Cyt *b₆f* in the mutants were due to data normalization on equal Chl basis. When normalized to leaf area, the content of Cyt *b₆f* was unaltered in *deap2-1* and *pam68-2* compared to WT, while PSII content was further reduced to 35% (Supplemental Table S3).

Together the quantification experiments performed on plants grown in low-light conditions show that PSII is the thylakoid complex that is most drastically affected by the loss of DEAP2 and that levels of all analyzed thylakoid membrane complexes are similarly affected in the *deap2-1* and *pam68-2* mutants.

Ribosome profiling reveals that loss of DEAP2 or PAM68 has mild but similar effects on chloroplast transcript accumulation and translation

Both DEAP2 and PAM68 are integral thylakoid proteins that are required for the accumulation particularly of PSII. To

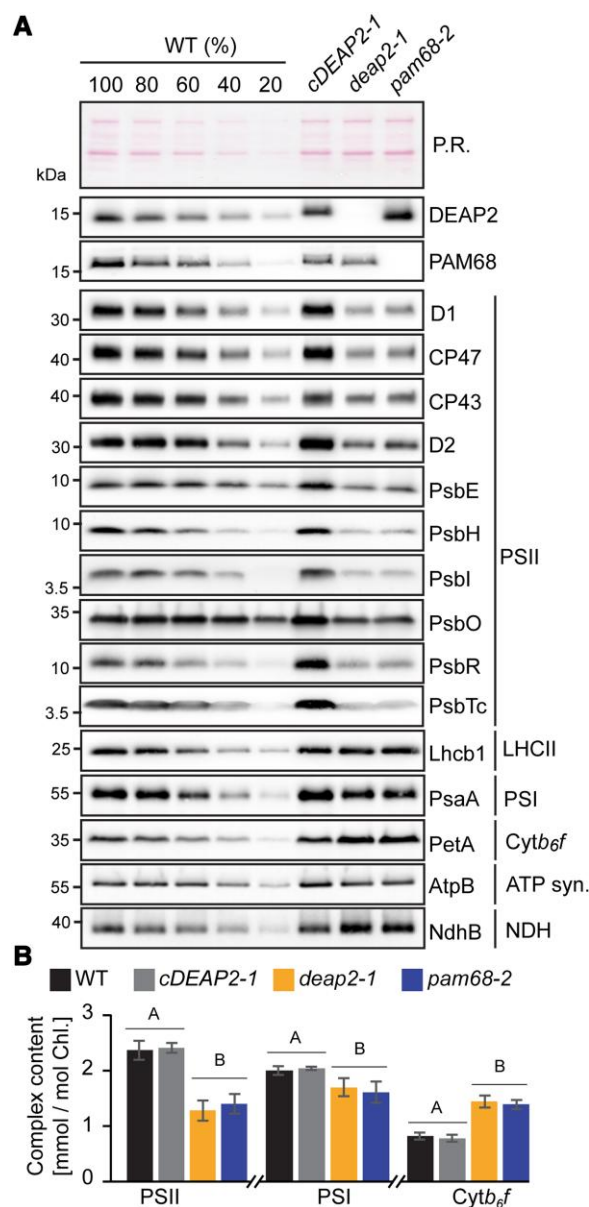


Figure 3. The *deap2* mutant contains similarly reduced PSII levels as *pam68*. **A)** Immunoblot analysis of thylakoid protein corresponding to the same amount of chlorophyll (Chl) from wild type (WT), *cDEAP2-1*, *deap2-1*, and *pam68-2* using specific antibodies against DEAP2 (1 μ g Chl) and PAM68 (5 μ g Chl), several subunits of photosystem II (PSII: D1, CP47, CP43, D2, PsbE, PsbH, PsbO, PsbR, PsbTc, all 1 μ g Chl and PsbI, 5 μ g Chl) and representative subunits of light-harvesting complex II (LHClI: Lhcb1, 1 μ g Chl), photosystem I (PSI: PsaA, 1 μ g Chl), cytochrome *b₆f* complex (Cyt: PetA, 1 μ g Chl), ATP synthase (AtpB, 1 μ g Chl), and NADPH-dehydrogenase complex (NDH: NdhB, 2 μ g Chl). Ponceau red (P.R.) served as a control for equal loading. Numbers left of the immunoblots indicate molecular weight in kDa of protein standards. **B)** PSII, PSI, and Cyt *b₆f* were quantified spectroscopically in isolated thylakoids relative to total chlorophyll. Averages are shown for $n = 5$ to $7 \pm$ SD. The capital letters above the graphs denote the two significantly different groups ($P < 0.05$) as determined by one-way ANOVA and Holm-Sidak multiple comparison test.

further investigate the function of both DEAP2 and PAM68 in the biogenesis of plant PSII and distinguish between potential effects on transcript accumulation and translation, we performed chloroplast ribosome profiling (Fig. 4A; Trösch et al. 2018). Changes in chloroplast RNA levels or ribosomal footprints (translation output) between mutants and WT were analyzed by a microarray-based method (see Materials and methods). All observed changes in transcript accumulation and translation output between the mutants and wild-type controls were below 2-fold indicating that neither DEAP2 nor PAM68 are likely to have a primary function in the expression of chloroplast-encoded PSII subunits or any other chloroplast gene (Fig. 3A, Supplemental Tables S4

to S7). The analysis of differential changes compared with WT by volcano plots (Supplemental Fig. S3) revealed a number of significant, below 2-fold differences that were very similar between *deap2-1* and *pam68-2*. On RNA level, both mutants showed significantly increased accumulation of *petB* and *petD* encoding for subunits of the Cyt *b₆f* complex, and decreased accumulation of *rbcL*. The calculation of translation efficiencies by normalizing translation output with RNA levels revealed a significant decrease for at least one subunit each of Cyt *b₆f* (*petA*), PSI (*psaA*, *psaB*), and the ATP synthase (*atpB*) in both mutants (for a schematic representation of common differences in both *deap2-1* and *pam68-2*, see Supplemental Fig. S4). PSII transcript accumulation was significantly upregulated in both mutants for *psbB* (CP47), *psbD* (D2), *psbH* and *psbT* (with *t*-test *P*-values <0.005), while translation efficiency was decreased for *psbF* and *psbH* compared with WT (with *t*-test *P*-values <0.02, Fig. 4B, Supplemental Table S7).

Together, the data reveal similar effects of the DEAP2 and PAM68 lesions on chloroplast transcript accumulation and translation. These effects were rather small, demonstrating that both proteins are not essential for transcription, transcript processing, or translation of chloroplast-encoded PSII subunits (or any other chloroplast gene). These comparably mild but common differences in transcript levels and translation efficiencies could be explained by regulatory feedback loops that are engaged to counteract the negative effects of both mutants on PSII accumulation. Here, the decrease in the translation efficiency of subunits encoding PSI and the ATP synthase may contribute to the lower accumulation of either complex in the thylakoid membrane of both mutants compared with WT (Fig. 3).

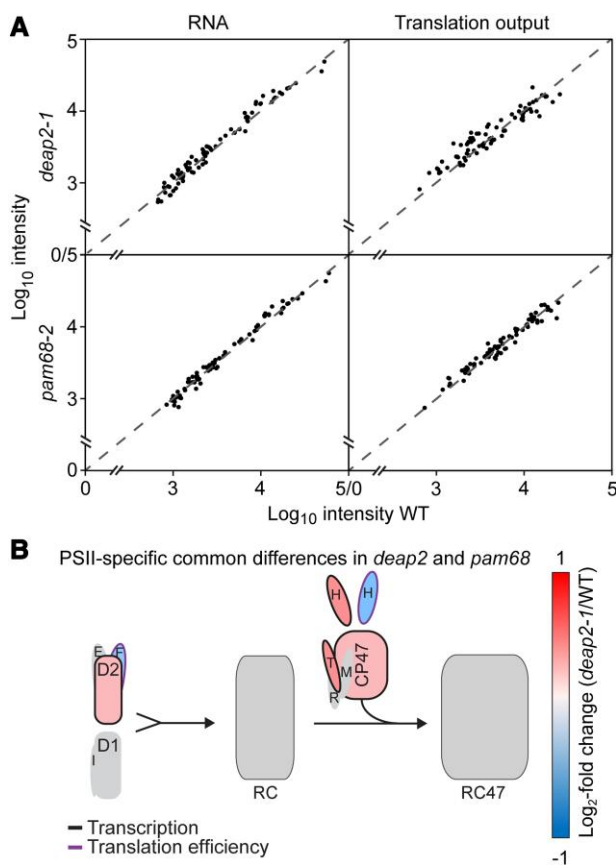


Figure 4. Levels of chloroplast-encoded transcripts and ribosomal footprints are slightly but similarly affected in *deap2* and *pam68* mutants. **A**) RNA (left) and ribosomal footprints (right, translation output) of chloroplast transcripts from rosettes of *deap2-1* (top) and *pam68-2* (bottom) relative to wild type (WT). All values, without any specific outliers, cluster around the dotted line, which signifies equal abundance in the mutant vs. WT. **B**) Graphical representation of common significant differences in both *deap2-1* and *pam68-2* mutants compared with WT for the different early steps of photosystem II (PSII) assembly on transcript levels (black outline, Student's *t*-test *P*-value < 0.005) or translation efficiency (purple outline, Student's *t*-test *P*-value < 0.02) (RC, reaction center assembly intermediate; RC47, assembly intermediate containing RC and the PSII intrinsic antenna CP47; single capital letters denote the respective PSII subunits).

DEAP2 affects PSII assembly similarly to PAM68 and is likewise not associated with PSII assembly intermediates

To obtain insight into thylakoid complex assembly in the *deap2* mutant and compare it with *pam68*, we solubilized thylakoid membrane protein complexes with *n*-dodecyl- β -D-maltoside (DDM) and fractionated them by blue-native (BN)-PAGE (Fig. 5A). Both WT and *cDEAP2-1* had a similar pattern of complex distributions with a strong blueish band at the expected size of monomeric PSII, running just above the Cyt *b₆f* dimer, a strong green band at the size of the PSI monomer and PSII dimer and a number of green bands corresponding to the high molecular mass PSII super-complexes (SC). These PSII-containing bands were all markedly and similarly reduced in the *deap2-1* and *pam68-2* mutants, while LHCII trimers were slightly increased. Next, complexes were fractionated into their subunits by SDS-PAGE and visualized by Coomassie staining.

This analysis supported the specific decrease of PSII, as only weak signals could be detected in the *deap2-1* and *pam68-1* mutants compared with WT and *cDEAP2-1* of the PSII core subunits D1, D2, CP43, and CP47 (Fig. 5, B to D,

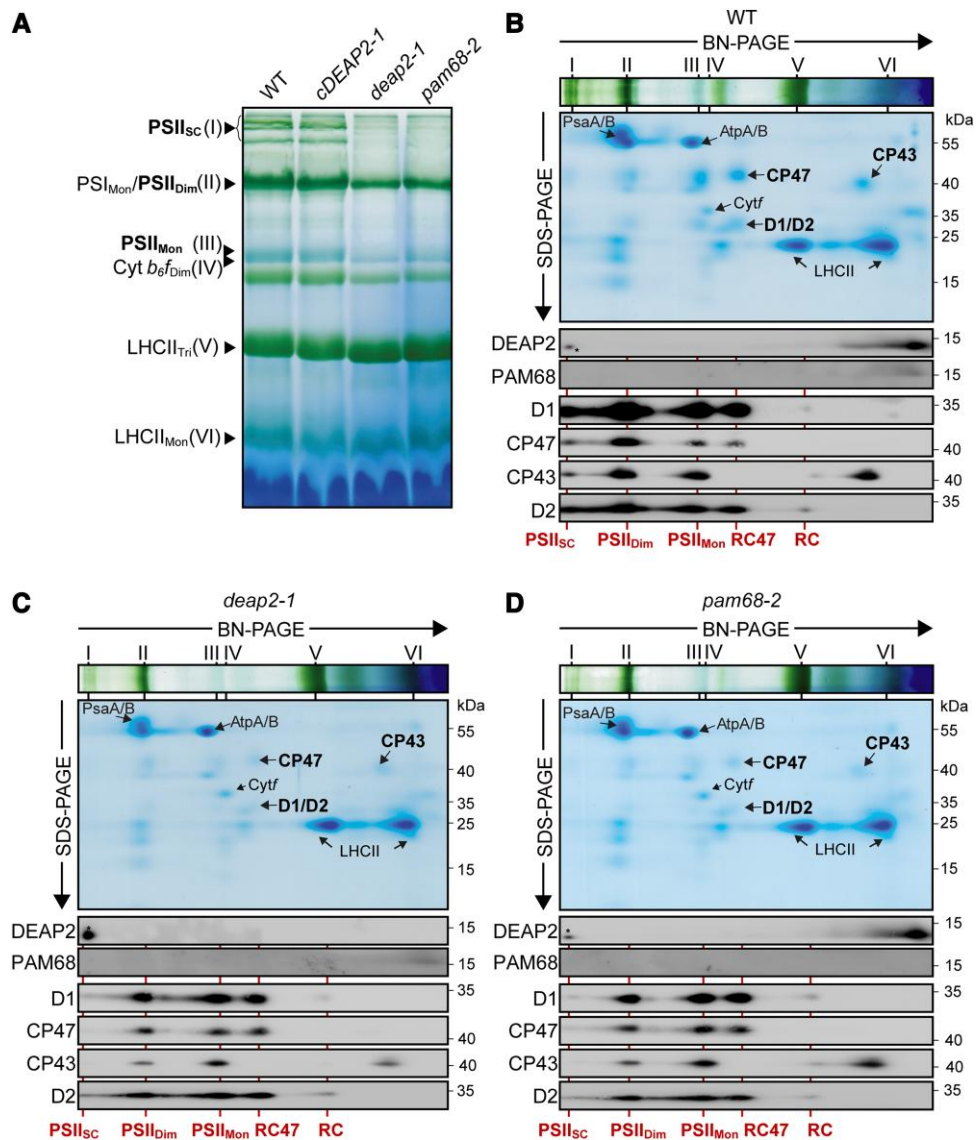


Figure 5. While the reaction center assembly intermediate accumulates to WT levels, higher molecular mass PSII assembly stages are reduced in *deap2* similar to *pam68-2*. **A**) Blue-native (BN)-PAGE analysis of thylakoid protein complexes. Thylakoid membranes of wild type (WT), *cDEAP2-1*, *deap2-1*, and *pam68-2* were solubilized with 1% (w/v) DDM at a concentration of 1 mg chlorophyll/ml and fractionated by BN-PAGE. Visible bands were assigned according to previous reports (Armbruster et al. 2010) and results shown below: photosystem (PS) II supercomplexes (PSII_{sc}; band I), PSI monomer and PSII dimer (PSI_{Mon}/PSII_{Di}; band II), PSII monomer (PSII_{Mon}; band III), dimeric cytochrome *b_f* complex (Cyt *b_f*_{Di}; band IV), trimeric light-harvesting complex (LHC) II (LHCII_{Tri}; band V), and monomeric LHCII (LHCII_{Mon}; band VI). PSII complexes are highlighted in bold. **B to D**) Thylakoid complexes fractionated according to size by blue native (BN)- of WT **B**), *deap2-1* **C**) and *pam68-2* **D**) were separated into their subunits by SDS-PAGE. The directions of separation from high to small molecular weight are indicated by the respective arrows. Gels were either stained with Coomassie or further processed for immunodetection of DEAP2, PAM68, and the PSII core proteins D1, CP47, CP43, and D2 using specific antibodies. Roman numerals on top of the BN-slices indicate complexes as shown in (A). Lines and labels below the panels indicate PSII assembly stages (RC, reaction center; RC47, RC + CP47). Numbers right of the immunoblots indicate molecular weight in kDa of protein standards. Asterisks indicate a cross-reaction of the DEAP2 antibody with a protein of slightly lower molecular mass found in high molecular weight complexes.

Supplemental Fig. S5). Additionally, immunoblot analyses were carried out on the BN second dimensions using specific antibodies against DEAP2 and PAM68 as well the four PSII core subunits D1, D2, CP43, and CP47. Both DEAP2 and PAM68 were mainly found to migrate as monomers or small molecular weight complexes and were not present in PSII complexes or its assembly intermediates. We found both

D1 and D2 to accumulate in WT and the mutant lines to similar levels in an early low abundant complex, which we assigned to the RC assembly intermediate. In accordance with the Coomassie-stained gels, levels of D1, D2, CP47, and CP43 were lower in both *deap2-1* and *pam68-2* compared with WT and *cDEAP2-1*. In both mutants, most signal of the PSII subunits was found in two assembly stages, one lacking CP43,

which we assigned to the RC47 assembly intermediate and the other one representing the PSII monomer. For WT and *cDEAP2-1*, the strongest signal was found in the PSII dimer and some also in PSII SC. Both knock-out mutants showed very little signal of PSII subunits in the PSII SC.

The 2D-BN-PAGE analysis revealed that DEAP2 like PAM68 does not comigrate with PSII assembly intermediates but is present in the thylakoid membrane as a monomer or in small molecular weight complexes. Both DEAP2 and PAM68 are required for the full accumulation of PSII assembly intermediates downstream of the RC, particularly for the final functional complexes, the PSII dimer and SC. Together, the results strongly support that DEAP2 has a function in PSII assembly, potentially at the same step as PAM68, which was shown to be the assembly of RC47 from RC (Armbruster et al. 2010).

Both DEAP2 and PAM68 are required for the formation of RC47 from RC

To monitor the dynamics of PSII assembly, we labeled newly synthesized chloroplast-encoded proteins radioactively. For this, discs of young leaves of WT, *deap2-1* and *pam68-2* (see Supplemental Fig. S6 for more details) were first infiltrated with cycloheximide to block cytosolic translation, then with

^{35}S -labeled methionine and floated on infiltration medium at low-light intensity for 20 min. From half of the leaf discs, thylakoids were isolated (pulse), while the second half was washed and infiltrated with nonlabeled methionine and incubated in low light for another 20 min before isolation of thylakoid membranes (chase). Thylakoid protein complexes were solubilized using DDM, separated by 2D-BN-PAGE and the radioactive signal of labeled proteins was detected (Fig. 6A).

In WT, mainly D1/D2, CP43, and CP47 were labeled with similar amounts in all respective PSII assembly stages after the pulse. After the nonradioactive chase, the signal of the RC intermediate was nearly gone and more label was found in the PSII assembly stages of higher molecular mass. In both the *deap2-1* and the *pam68-1* mutants, we found that the RC D1/D2 signal was comparable to WT after the pulse. Only very few label was observable in further higher molecular mass PSII assembly stages in these mutants. In contrast to WT, the nonradioactive chase did not greatly deplete the level of label in the RC and signal in the higher molecular weight complexes remained low.

Together, these analyses reveal that *deap2-1* and *pam68-2* show identical defects in the dynamics of PSII assembly. Loss of either protein dramatically impairs the process downstream of the RC formation (Fig. 6B).

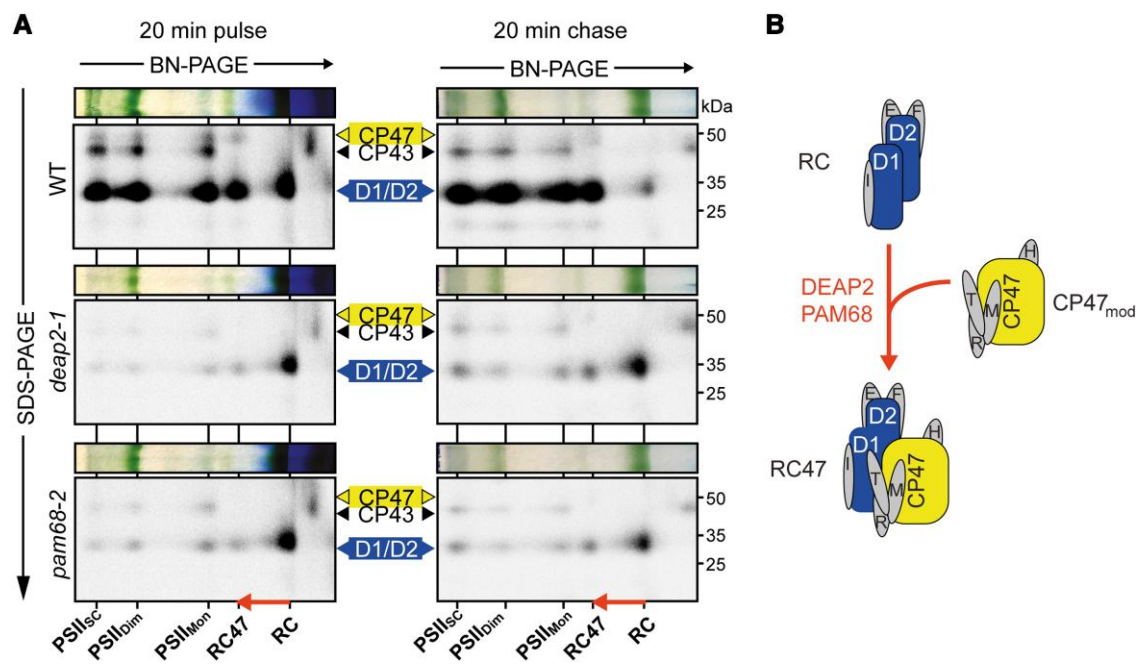


Figure 6. PSII assembly in *deap2* stalls at the RC stage exactly as in *pam68*. **A**) Analysis of the dynamics of photosystem II (PSII) assembly by labeling newly synthesized chloroplast proteins with [^{35}S] methionine and separating thylakoid complexes and denatured subunits by 2D blue-native (BN) gel electrophoresis. Leaf discs from wild type (WT), *deap2-1* and *pam68-2* were pulse labeled for 20 min in the presence of cycloheximide and thylakoids were directly processed, or leaf discs were first infiltrated again with nonradioactive methionine to be able to chase [^{35}S] methionine incorporation into higher PSII assembly stages [supercomplexes (PSII_{SC}), dimers (PSII_{D1}), monomers (PSII_{Mon}), reaction center (RC) and RC + CP47 (RC47)]. The arrow shows the transition from the RC to the RC47 assembly intermediates. Numbers right of the autoradiographs indicate molecular weight in kDa of protein standards. **B**) Scheme illustrating the transition from RC to RC47, of which efficient processing is dependent on the presence of both DEAP2 and PAM68.

Plants that lack both DEAP2 and PAM68 cannot make functional PSII

Because loss of DEAP2 has a comparable effect on PSII assembly as loss of PAM68, we investigated the possibility that both proteins act cooperatively in this process. For this, we generated double mutants of *deap2-1* and *pam68-2*. No double mutants were identified from F2 plants grown on soil, suggesting that these plants could not grow photoautotrophically. Thus, the selection was continued on sucrose-containing agar plates and double mutants could be isolated. These plants were white, small and had no measurable Fv/Fm (Fig. 7A), indicating that plants lost the capacity to grow photoautotrophically, because they lacked PSII. To confirm this, immunoblot analyses were performed on total protein extracted from leaf discs of WT, single mutants and the *deap2-1 pam68-2* double mutant (Fig. 7B). While the content of the Actin control was comparable between the genotypes, PSII subunits were below detection level in the *deap2-1 pam68-2* double mutant. Analyzed subunits for the Cyt *b₆f* complex, PSI and ATP synthase were lower as compared to single *deap2-1* and *pam68-2* mutants but were detectable at around 50% of WT. Thus, other thylakoid complexes accumulated to much higher levels than PSII in the double mutant, supporting that PSII assembly is the main defect in the double mutant. To control for the specificity of this identified genetic interaction between *deap2* and *pam68*, we additionally crossed *pam68-2* with *lpa1-2*, a mutant with impaired integration of D1 in the thylakoid membrane. These double mutants displayed an intermediate Fv/Fm value between the slightly lower *pam68-2* and higher *lpa1-2* (Supplemental Fig. S7, A and B). The loss of both PAM68 and LPA1 in these plants was confirmed by immunoblotting using specific antibodies against both proteins (Supplemental Fig. S7C).

Together, the data demonstrate that the simultaneous absence of DEAP2 and PAM68 leads to a complete disruption of PSII assembly. Possible explanations for this could be a cooperative or a redundant function of the two proteins during the assembly of RC47 from RC and the CP47 module.

DEAP2 overexpression can partially rescue the loss of PAM68 but not vice versa

To further test for a potential redundancy of DEAP2 and PAM68 in the PSII assembly process, we generated mutant lines, in which the other protein was overexpressed as a Myc-tagged version. As a control, we additionally generated PAM68 overexpression plants in the *pam68-2* background. From five positive transformants each, as detected by the Myc antibody, we selected three with varying levels of overexpression and performed further experiments on the two with the lowest and highest expression (Fig. 8A, Supplemental Fig. S8).

Overexpression of PAM68 in *pam68-2* complemented the low growth and Fv/Fm phenotype but did not have any effects in *deap2-1*, while overexpression of DEAP2 in the *pam68-2* rescued these two phenotypes to some degree (Fig. 8, B and C). These *pam68-2* plants with 2-fold increased

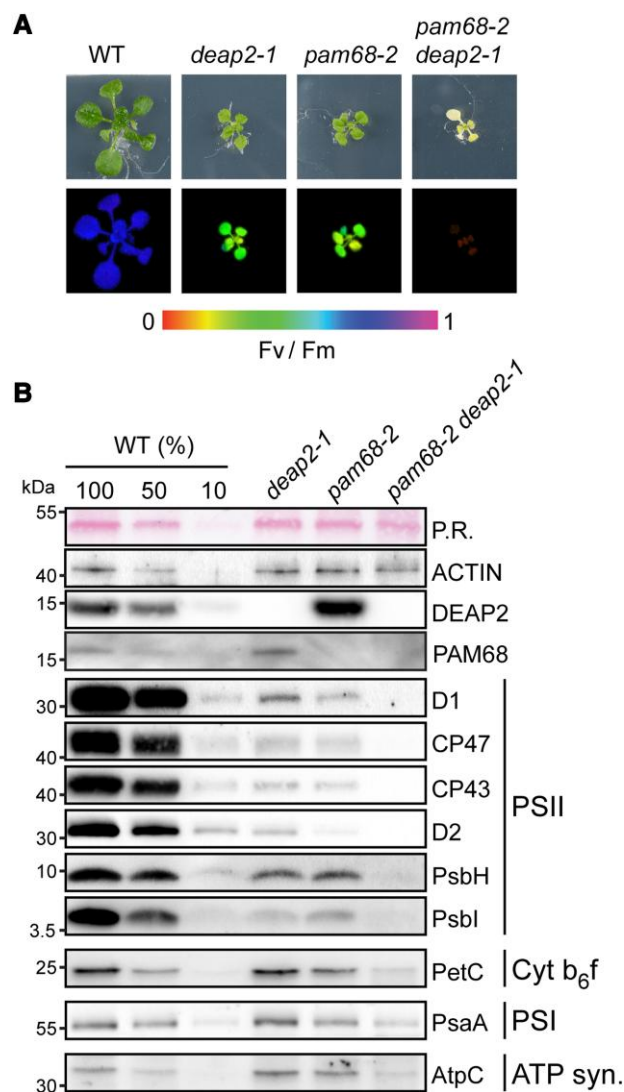


Figure 7. Plants lacking both DEAP2 and PAM68 do not accumulate any functional PSII. **A**) Plants lacking both DEAP2 and PAM68 (cross of *pam68-2* and *deap2-1*) are only viable on MS medium supplemented with 2% (w/v) sucrose. Pictures (upper panel) and false color maximum photosystem (PS) II quantum yield (Fv/Fm) images (lower panel) of 4-week-old wild type (WT), *deap2-1*, *pam68-2*, and *pam68-2 deap2-1* double mutants grown at 50 $\mu\text{mol photons m}^{-2} \text{s}^{-1}$ and 12 h/12 h dark light cycles. Signal intensities for Fv/Fm were calculated from chlorophyll fluorescence analyses and are given by the false color scale below the panels. **B**) Immunoblot analysis of total protein extracts from plants as in (A). Samples were fractionated by SDS-PAGE and blots were probed with specific antibodies against DEAP2, PAM68, several subunits of PSII (D1, CP47, CP43, D2, PsbH, PsbI), Cyt *b₆f* (PetC), PSI (PsaA), and the ATP synthase (AtpC). Ponceau red (P.R.) stained RbcL on the membrane before detection and Actin were used to control for equal protein loading. Numbers left of the immunoblots indicate molecular weight in kDa of protein standards.

levels of DEAP2 had significantly higher Fv/Fm and larger leaf area compared with *pam68-2* alone. To investigate whether this was due to higher levels of PSII accumulating in the *pam68-2* 35S:DEAP2 lines, we performed immunoblot

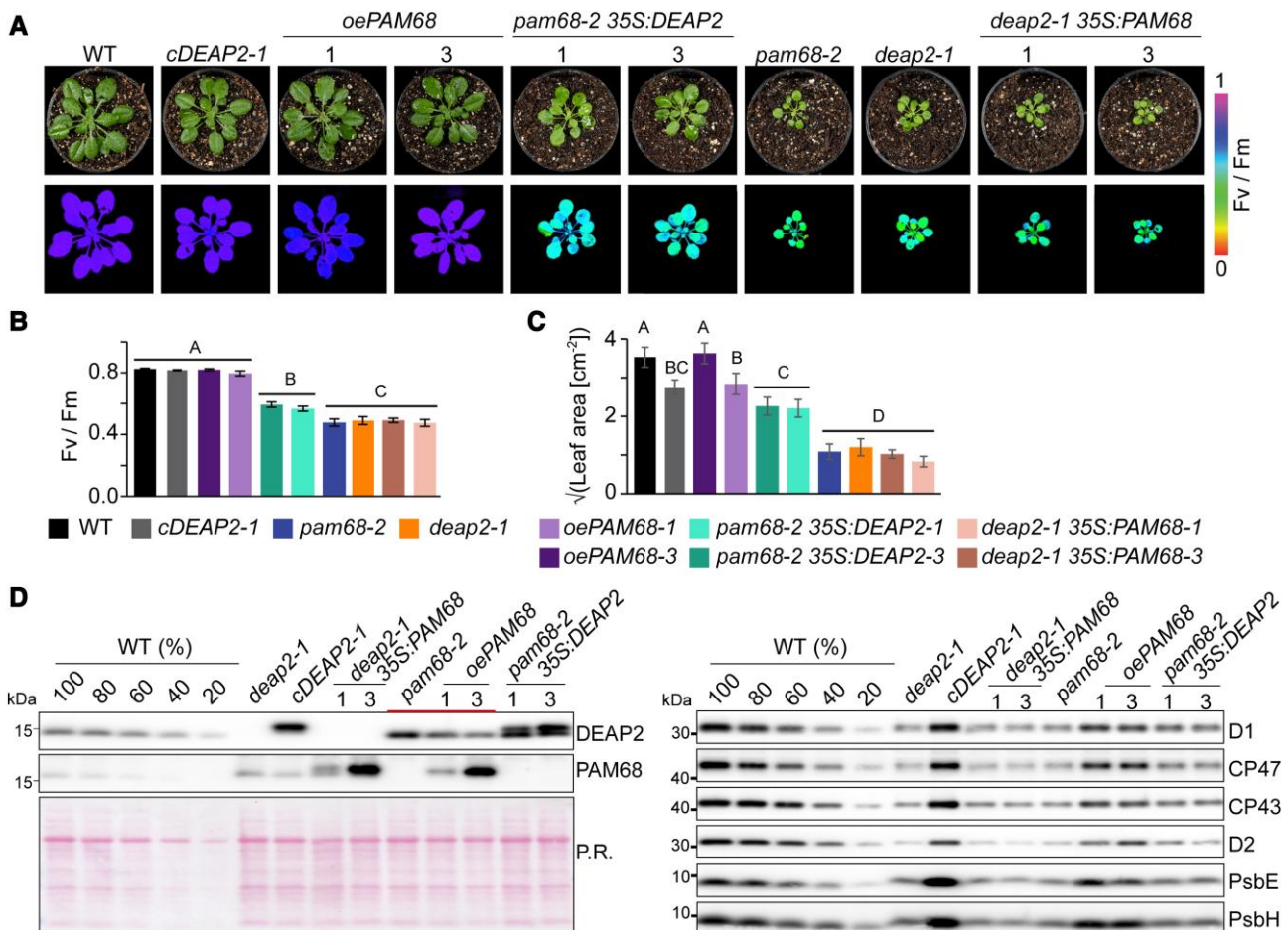


Figure 8. DEAP2 can partially compensate for loss of PAM68 but not vice versa. **A**) Pictures (upper panel) and false color images of the maximum quantum yield of photosystem (PS)II (Fv/Fm, lower panel) of 6-week-old wild type (WT), *deap2-1*, *cDEAP2-1*, *pam68-2*, *deap2-1* overexpressing PAM68 (*deap2-1 35S:PAM68*), *pam68-2* overexpressing PAM68 (*oePAM68*) or DEAP2 (*pam68-2 35S:DEAP2*). All overexpressed proteins carry a c-terminal MYC-tag. Three independent lines with varying amounts of protein expression were selected (Supplemental Fig. 7). Shown here are lines #1 and #3 with lowest and highest Myc-tagged protein levels as determined by immunoblotting. Signal intensities for Fv/Fm were calculated from chlorophyll fluorescence analyses and are reflected by the false color scale beside the panels. **B and C**) Fv/Fm (B) and leaf area (C, shown as square root) from $n = 6–10$ genotypes as shown in (A) with error bars indicating standard deviation. Capital letters above graphs indicate groups with significant differences between genotypes ($P < 0.05$) as determined by one-way ANOVA and Holm-Sidak multiple comparison test. **D**) Immunoblot analysis of total protein extracts using specific antibodies against DEAP2 and PAM68 (left panel) and PSII subunits (right panel). The accumulation of subunits of other thylakoid complexes is shown in Supplemental Fig. 7. Ponceau red (P.R.) staining of one membrane prior to immunodetection is shown as a loading control. The additional thick line in the left panel indicates plant lines with varying PAM68 levels, revealing the inverse response of DEAP2 accumulation.

analyses on multiple subunits and observed generally a slight increase compared with *pam68-2* (Fig. 8D). By comparing the signals of DEAP2 and PAM68 in the different lines, we observed that DEAP2 decreased with increasing PAM68 levels.

To obtain information about the relationship between DEAP2 and PAM68 on protein level, we quantified their relative abundances (Fig. 9A). For equal amounts of Myc-tagged protein, we loaded $1\times$ *cDEAP2-1*, which had similar DEAP2 levels as WT (Supplemental Fig. S9), and $4\times$ *oePAM68-3*, which had 5-fold higher PAM68 levels than WT (Supplemental Figs. S8 and S9). This result shows that DEAP2 is $\sim 20\times$ more abundant than the PAM68.

Discussion

DEAP2 is a eukaryote-specific factor that cooperates with PAM68 in the progression of the RC to the RC47 PSII assembly intermediate

This study has uncovered DEAP2 as a PSII assembly factor, which together with the known assembly factor PAM68 facilitates the formation of the RC47 intermediate from RC and the CP47 module. We revealed that the lack of DEAP2 and PAM68 have nearly identical effects on all stages of thylakoid biogenesis and PSII assembly. Both the *deap2* and *pam68* mutants show comparable defects in the accumulation of thylakoid complexes with a strong reduction in PSII

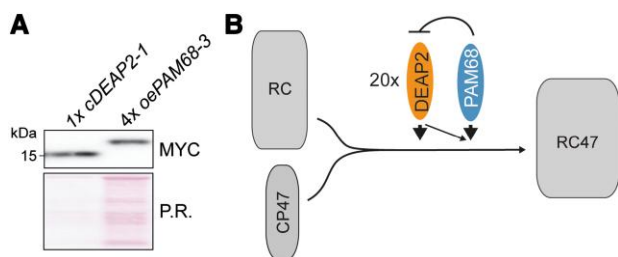


Figure 9. DEAP2 has 20-fold higher protein levels than PAM68 and model of function. **A)** Quantification of relative PAM68 and DEAP2 levels. Total protein extracts of $1\times$ *cDEAP2-1* (corresponding to the same wild-type (WT) amount) and $4\times$ *oePAM68-3* (5-fold overexpression) yield the same Myc signal. Ponceau red (P.R.) staining of one membrane prior to immunodetection is shown as a loading control. **B)** Schematic model of the transition from reaction center (RC) PSII assembly stage to the RC + CP47 (RC47) intermediate. This assembly step is facilitated by DEAP2 and PAM68, whereby DEAP2 is 20-fold more abundant than PAM68. Increasing PAM68 levels lead to decreasing DEAP2 accumulation and higher amounts DEAP2 can partially compensate for lack of PAM68.

subunits and assembled PSII dimers as well as supercomplexes (Figs. 3 and 5). Decreases in the levels of PSI and the ATP synthase in the mutants compared with WT can be explained by the downregulation of some of their subunits at the translational level, potentially involving a negative feedback loop in response to low PSII accumulation (Fig. 4). Consistent with this, it has previously been shown that many PSII biogenesis mutants with pronounced reductions in their PSII content display a parallel, but milder decrease in PSI levels. For example, in tobacco (*Nicotiana tabacum*) mutants with reduced *psbD* mRNA abundance, a decrease in PSII content to 20% of wild-type levels resulted in a reduction of PSI content to 35% of wild-type levels (Fu et al. 2021). Also, Arabidopsis mutants specifically affected in PSII assembly show a concomitant reduction in PSI accumulation (Meurer et al. 1998; Peng et al. 2006; Link et al. 2012; Li et al. 2019). Together, this further supports that the decreased PSI content observed here is a consequence of altered PSII abundance, and not attributable to any additional function of DEAP2 or PAM68 related to PSI.

PSII assembly of both mutants is impaired at the RC assembly intermediate. Lack of either protein strongly decreases the progression from RC to RC47. The PAM68 ortholog in cyanobacteria was previously shown to interact with ribosomes and proposed to promote CP47 synthesis and cotranslational insertion of Chl molecules (Bučinská et al. 2018). Such a function of PAM68 could explain why the assembly process is slowed down at the RC also in plants. However, the incorporation of radioactive label into newly synthesized thylakoid CP47 protein was not affected in plants lacking PAM68 (Armbruster et al. 2010). The ribosome profiling analyses of this report again argue against an effect of Arabidopsis PAM68 on the overall synthesis of CP47, as we

could not observe any differences in *psbB* translation efficiencies between WT and *pam68* (Fig. 4, Supplemental Fig. S3 and Tables S6 to S7). Instead, we found a decrease in the *psbH* translation efficiencies in both mutants, which may indicate a function of these proteins related to the assembly of PsbH together with CP47. For cyanobacteria, it was previously suggested that PsbH shares the same CP47 binding site with PAM68 and replaces PAM68 after the insertion of Chl into CP47 (Bučinská et al. 2018).

Together, our results suggest that the assembly of RC47 from the RC intermediate is not as highly conserved between plants and cyanobacteria as previously thought. While both, cyanobacteria and plants, require the PAM68 protein for the efficient progression of this PSII assembly step, plants additionally engage the DEAP2 protein. DEAP2 represents a eukaryotic addition as orthologs are absent in cyanobacterial genomes (Karpowicz et al. 2011). Further research is needed to pin point evolutionary differences in the assembly of RC47 that lead to the requirement for DEAP2 in plants. Whether this includes adjustments to the molecular function of PAM68 requires careful elucidation by comparative analyses.

DEAP2 and PAM68 appear to have complementary functions

We demonstrate that DEAP2 can at least partially compensate for the loss of PAM68 but not vice versa. The 2-fold amplification of DEAP2 levels in the *pam68* background by expression of a second DEAP2 copy from the 35S promoter, partially rescued the low Fv/Fm and growth phenotypes of the *pam68* mutant (Fig. 8B). However, particularly PSII subunit accumulation and Fv/Fm as a read-out for functional PSII were still strongly reduced compared with WT, demonstrating that even when DEAP2 is present in excess, PAM68 is still required for an efficient PSII assembly process. Given that DEAP2 is 20 times more abundant than PAM68 (Fig. 9), this points to a function of PAM68 which cannot be entirely replaced with DEAP2. Our results rather suggest that an excess of DEAP2 buffers against the negative consequences that loss of PAM68 has on PSII assembly. The absence of functional PSII assembly in the double mutant is also consistent with this hypothesis. A 4-fold excess of PAM68 cannot ameliorate the negative effects of DEAP2 loss on PSII functionality. This may be due to overexpressed PAM68 being present in substoichiometric amounts compared with DEAP2 and thus not accumulating to high enough levels for entirely taking over the function of DEAP2. In this case, however, we would expect at least a partial rescue of the *deap2* phenotype by PAM68 overexpression, which is not the case. The inability of PAM68 overaccumulation to compensate for the loss of DEAP2 rather supports the hypothesis that both proteins have distinct functions. Interestingly, levels of DEAP2 appeared to decrease with increasing PAM68 levels (Fig. 8D). A 4-fold increase in PAM68 caused a slight decrease in DEAP2 levels up to 80% of WT. In line with the 20 times higher levels of DEAP2 in the thylakoid membrane compared

with PAM68, this may suggest a stoichiometric destabilizing effect of PAM68 on DEAP2. The instability of a larger pool of DEAP2 is supported by the observation that *deap2-1* plants overexpressing DEAP2 from the 35S promoter can only accumulate WT levels of DEAP2. Also, in *pam68-2* mutants, DEAP2 levels only reach a maximum of 2-fold compared with WT.

Conclusion

While multiple PSII assembly factors have been reported, exact mechanistic insight into how most of these factors promote PSII biogenesis is still lacking. This study paves the way for further investigations into how (i) RC47 assembly differs between cyanobacteria and plants and (ii) DEAP2 and PAM68 contribute to this process mechanistically. In particular, molecular understanding of how DEAP2 stabilizes the transition from RC to RC47 even in the absence of PAM68 may reveal strategies to enhance and accelerate the safe assembly of plant PSII, but potentially also other multipartite complexes with highly reactive cofactors.

Materials and methods

Plant material and growth conditions

The Salk T-DNA *Arabidopsis* (*A. thaliana*) insertion lines *deap2-1* (SALK_048033), *pam68-2* (SALK_044323; Armbruster et al. 2010), *lpa1* (SALK_124398), herein referred to as *lpa1-2*, were obtained from NASC (Alonso et al. 2003) and genotyped using specific primers. The insertion in *deap2-1* was confirmed by sequencing the flanking region of the insertion. To generate plant expression constructs, the *DEAP2* or *PAM68* coding regions were amplified from cDNA using gene-specific primers adding a sequence encoding for a C-terminal MYC-tag and inserted into the binary vector pEarleyGate100 (pEG100; Earley et al. 2006) linearized with *Xba*I and *Xho*I restriction enzymes downstream of the 35S promoter by using Gibson Assembly (Gibson et al. 2009). Additionally, the *DEAP2* cDNA and the sequence encoding for YFP were introduced into pEG100 in the same way to obtain a protein fusion of DEAP2 to YFP at its C-terminus. Primers used for genotyping and cloning can be found in Supplemental Table S8. Homozygous *deap2-1* and *pam68-2* plants were transformed by floral dip as described previously (Clough and Bent 1998). Transgenic plants (*cDEAP2*, *oePAM68*, *deap2* 35S:PAM68, *pam68* 35S:DEAP2) were selected based on their resistance to BASTA, and expression of the fusion protein was detected by immunoblot analysis using an antibody against the Myc-tag.

Arabidopsis plants were grown in pots on soil (Stender, Schermbeck, Germany) containing 1 g/l Osmocote or on Murashige and Skoog medium with 0.8% agar (w/v) supplemented with 2% sucrose (w/v) at $\sim 50 \mu\text{mol photons m}^{-2} \text{ s}^{-1}$, 20 °C/16 °C, 60%/75% relative humidity in 12 h/12 h day/night cycles. Experiments on soil-grown plants were performed on 6- to 8-week-old WT, *cDEAP2*, *oePAM68* and 10- to 12-week-old

deap2-1, *pam68-2* as well as *deap2* 35S:PAM68 and *pam68* 35S:DEAP2.

Transient expression of DEAP2-YFP fusions in *Nicotiana benthamiana* leaves

The *Agrobacterium tumefaciens* strain GV3101 transformed with the DEAP2–YFP constructs was resuspended in the induction medium (10 mM MgCl₂, 10 mM MES-KOH pH 5.6, 150 μM acetosyringone) to an OD₆₀₀ of 0.5. After 2 h at 28 °C, suspensions were inoculated onto sections of well-watered *N. benthamiana* leaves by injecting into the bottom side (Blatt and Grefen 2014). Transfected plants were grown for 2 d before leaf discs were analyzed for the subcellular localization of the YFP fluorescence signal. For microscopy, the Leica TCS SP5 instrument was used with 63 \times /1.4 objective and water immersion. Fluorophores were excited by using an argon laser (intensity: 20%) at 514 nm, YFP fluorescence was detected between 524 and 582 nm, and Chl fluorescence between 618 and 800 nm (gain settings: PMT 5, 660 V; PMT-Trans, 436 V).

In silico analyses

Sequence alignment and phylogenetic reconstructions were done using ClustalW (<https://www.genome.jp/tools-bin/clustalw>). Sequences were retrieved from Phytozome v13 (<https://phytozome-next.jgi.doe.gov>). The protein alignment and phylogenetic reconstructions were performed using Clustal Omega and default settings (<https://www.ebi.ac.uk/Tools/msa/clustalo>). The tree was viewed from the resulting Newick format file using NCBI's Tree Viewer (<https://www.ncbi.nlm.nih.gov/projects/treeview>). The *Arabidopsis* DEAP2 chloroplast transit peptide (cTP) and transmembrane domains were predicted using TargetP (Armenteros et al. 2019) and DeepTM HMM (Hallgren et al. 2022), respectively. The protein structure of DEAP2 (without cTP) was predicted by AlphaFold (Jumper et al. 2021) or I-TASSER (Zhou et al. 2022), and overlaid using PyMols *super* function (<http://www.pymol.org/pymol>). The I-TASSER model quality was evaluated by estimated RMSD, estimated TM-score, structural alignments against known protein structures from PDB and the I-TASSER own quality parameter C-score. Additionally, the online tool MolProbity (Davis et al. 2007) was used for stereo-chemical quality (Ramachandran) analysis of all predicted models.

Protein isolation, gel electrophoresis, and immunodetection

Total protein was extracted from pulverized leaf material using sample buffer (0.1 M Tris pH 6.8, 24% glycerol (v/v), 8% SDS (w/v), 5% mercapto-ethanol (v/v), 0.02% bromophenol blue (w/v)) and heating at 40 °C for 30 min. Thylakoid membranes were isolated as described previously (Armbruster et al. 2014). Total Chl content and a/b ratio were measured in 80% (v/v) acetone according to Porra et al. (1989). For SDS PAGE, total protein extracts or thylakoid samples incubated with sample buffer were resolved

on a 16% (w/v) polyacrylamide gel containing 4 M urea (Schägger 2006). For BN-PAGE, thylakoid membranes at a concentration equal to 1 mg of total Chl/mL were solubilized with 1% (w/v) β -n-dodecyl-d-maltoside (DDM), and separated on a 6–12% (w/v) polyacrylamide gradient gel according to Peng et al. (2008). The BN-PAGE was further fractionated by SDS-PAGE. For this, BN-PAGE gel strips were first incubated with 66 mM Na_2CO_3 , 2% SDS (w/v) and 50 mM DTT at 50 °C for 30 min to denature proteins. After electrophoresis, gels were either stained with Coomassie blue (R-250, 40% (v/v) methanol, 7% (v/v) acetic acid, 0.05% (w/v) Coomassie blue R-250) or used for immunoblotting analyses. For immunoblot analyses with specific antibodies, gels were blotted onto nitrocellulose and visualized with Ponceau Red (0.1% Ponceau S (w/v) in 5% (v/v) acetic acid) prior to immunodetection. Membranes were blocked with 50 mM Tris, 10 mM NaCl, 0.05% (v/v) Tween 20, 0.2% (v/v) Triton X-100% and 5% (w/v) nonfat dry milk and incubated with antibodies against D1 (AS10704), CP47 (AS04038), CP43 (AS111787), D2 (AS06146), PsbE (AS06112), PsbH (AS06157), PsbI (AS06158), PsbO (AS06142-33), PsbR (AS05059), Lhcb1 (AS01004), Lhcb2 (AS01003), PsaA (AS06172), PetA (AS06119), PetC (AS08330), AtpB (AS05085), AtpC (AS08312), RbcL (AS03037), NdhB (AS164064), Tic40 (AS10709), Actin (AS214615-10), and Myc (AS153034), all obtained from Agrisera (Sweden), as well as PAM68 (PHY2289A) and PsbTc (PHY0350A) obtained from PhytoAB and diluted according to manufacturer's instructions. For immunodetection of DEAP2, an antibody was produced by Pineda Antikörper-Service (Germany) targeting the C-terminal end of the protein (peptide sequence: VEAANKEAQEQDKRDGFL) and diluted 1:1,000. For secondary antibodies coupled to the horse-radish peroxidase, a mouse- or rabbit-specific antibody was used from Agrisera (against Actin; AS09627) or Sigma-Aldrich (A8275), respectively, at a dilution of 1:10,000. Signals were detected using the SuperSignal West Femto Chemiluminescence-substrate (ThermoFisher) and the G-Box-ChemiXT4 (Syngene) or the C-DiGit Blot Scanner (Li-Cor).

Chloroplast isolation, fractionation, and chaotropic salt treatment of isolated thylakoids

Intact Arabidopsis chloroplasts were isolated via a two-step Percoll gradient centrifugation (Kunst 1998). In brief, the homogenized leaf tissue was fractionated on the gradient and intact chloroplasts were collected from the interphase. Chloroplasts were fractionated into envelope, thylakoids, and stroma via a three-step sucrose gradient centrifugation after being hypotonically lysed in 10 mM Tris/HCl, pH 8.0 and 1 mM EDTA, pH 8.0, at a Chl concentration of 2 mg/mL (Li et al. 1991). For salt washes of thylakoids, isolated thylakoids were resuspended in 50 mM HEPES/KOH, pH 7.5, at a Chl concentration of 0.5 mg/mL (Karnauchov et al. 1997). Extraction with 2 M NaCl, 0.1 M Na_2CO_3 , 2 M NaSCN, or 0.1 M NaOH was performed for 30 min on ice, soluble and membrane proteins were separated by centrifugation for 10 min at 10,000 g and

4 °C, and immunoblot analysis was performed on both fractions.

Spectroscopic plant analysis and photosynthetic complex quantification

The MAXI IMAGING-PAM (Walz, Effeltrich, Germany) was used for Chl *a* fluorescence analysis. Minimal fluorescence F_0 , and maximal fluorescence F_m of 30 min dark-acclimated plants were measured before and during the application of a 0.8 s saturating light pulse, respectively. The maximum yield of PSII F_v/F_m was calculated as $(F_m - F_0)/F_m$. PSI measurements were performed with the plastocyanin-P700 version of the Dual-PAM instrument (Schöttler et al. 2007), which allows the deconvolution of absorbance changes arising from plastocyanin and PSI. Plants were directly taken from the controlled environment chambers and measured without dark adaptation. The quantum yield of nonphotochemical energy dissipation due to donor side limitation of PSI ($Y(\text{ND})$) was determined according to (Schreiber and Klughammer 2016). All measurements were performed in the middle of the light period.

Thylakoid membranes were isolated as previously described (Schöttler et al. 2004). The contents of PSII and the Cyt b_6/f were determined from difference absorbance signals of Cyt b_{559} (PSII) and the cytochromes b_6 and f , respectively. To improve the optical properties of the samples, thylakoids equivalent to 50 μg Chl mL^{-1} were destacked in low-salt medium supplemented with 0.03% (w/v) DDM (Kirchhoff et al. 2002). All cytochromes were fully oxidized by the addition of 1 mM potassium hexacyanoferrate (III). Then, 10 mM sodium ascorbate was added to reduce the high-potential form of cyt b_{559} and cytochrome f . Finally, the addition of 10 mM sodium dithionite reduced the low potential form of cyt b_{559} and the two b-type hemes of cytochrome b_6 . Using a V-750 spectrophotometer equipped with a custom-made head-on photomultiplier (Jasco GmbH, Pfungstadt, Germany), at each of the three redox conditions, 10 absorbance spectra were measured between 575 and 540 nm with a spectral bandwidth of 1 nm and a scanning speed of 100 nm min^{-1} , and subsequently averaged. Difference spectra were calculated by subtracting the spectrum measured in the presence of hexacyanoferrate from the ascorbate spectrum, and by subtracting the ascorbate spectrum from the spectrum measured in the presence of dithionite, respectively. Finally, a baseline calculated between 540 and 575 nm was subtracted from the signals. Then, the difference spectra were deconvoluted as previously described (Kirchhoff et al. 2002). PSI was quantified from light-induced difference absorbance changes of P_{700} . Thylakoids equivalent to 50 μg Chl mL^{-1} were solubilized in the presence of 0.2% (w/v) DDM. After the addition of 10 mM sodium ascorbate as electron donor and 100 μM methylviologen as electron acceptor, P_{700} was fully photooxidized by applying a light pulse (250 ms length, 2000 $\mu\text{mol photons m}^{-2} \text{s}^{-1}$ intensity). Measurements were performed with the Pc-P700 version of the Dual-PAM instrument (Heinz Walz GmbH). Finally, based on the Chl content

of the investigated leaves, all complex contents were renormalized to a leaf area basis. Results were analyzed using one-way ANOVA and Holm-Sidak multiple comparison test to determine the statistical significances between genotypes.

Immunoprecipitation of DEAP2 and following MS analysis

Thylakoids were solubilized in 50 mM HEPES pH 8.0; 330 mM sorbitol; 150 mM NaCl; 4 mM PMSF containing 1% (w/v) β -DM for 10 min on ice. The supernatant was recovered after centrifugation and incubated with magnetic beads at 4 °C overnight. Beads that were made specific for DEAP2 by attaching the antibody to Protein G-coupled beads (Dynabeads, ThermoFisher) according to protocol, or Myc-antibody coupled beads (Myc-trap, ChromoTek) were used. After incubation, the beads were washed five times with the same buffer containing 0.2% (w/v) β -DM, before samples were further processed. For MS analysis, proteins were reduced with TCEP, alkylated with chloroacetamide, and digested with trypsin for 14 h at 37 °C. The peptide mixture was purified and desalted on C₁₈ SEP-Pak columns (Waters). Measurements were performed on a Q Exactive HF or Exploris 480 mass spectrometer coupled with a nLC1200 nano-HPLC (Thermo Scientific). Quantitative analysis of MS/MS measurements was performed with the MaxQuant software (Cox and Mann 2008) and the Andromeda search engine was used to annotate peptide sequences using the Arabidopsis TAIR10 genome annotation database.

Ribosome profiling

Plant material was harvested 1 h after the start of the photo-period from 6-week- (WT) and 10-week- (mutants) old plants (at comparable developmental stage), immediately frozen in liquid nitrogen and stored at –80 °C until further processing. For each line, three replicates were used, consisting of 10 independent plants. The ribosome profiling was done as previously described (Zoschke and Barkan 2015; Trösch et al. 2018).

Ribosome footprints and total RNA were prepared, labeled, and hybridized as described previously (Trösch et al. 2018; Schuster et al. 2020; Ghandour et al. 2023). Briefly, 4 μ g ribosome footprint RNA and 3.5 μ g total RNA from *deap2-1*, *pam68-2* and wild-type plants were chemically labeled with Cy3 and Cy5, respectively, and hybridized onto identical custom microarrays as described (Trösch et al. 2018). These microarrays contain 50-nt probes that cover chloroplast protein-coding regions and UTRs in high density (one 50mer probe starting every 30 nt within these regions; each probe is represented in four technical replicate spots on each microarray). Transcript and ribosome profiling data were processed as described previously (Schuster et al. 2020; Gao et al. 2022). In brief, background-subtracted probe signals lower than 100 were set to zero. Probes that showed signal saturation were excluded from further analysis. Signal intensities of all probes covering protein-coding regions (in

all experiments and replicates) were normalized to the average signal intensities of probes covering protein-coding regions in the three wild-type datasets (Supplemental Tables S4 and S5). For each chloroplast reading frame, the average signal intensity values based on the signal intensities of all probes located in a given reading frame was calculated to determine the fold-change differences in comparison to wild-type data. Significances of changes in gene expression were calculated by Student's *t*-test and the derived *P*-values were adjusted for multiple testing as described previously (Benjamini and Hochberg 1995).

In vivo labeling of newly synthesized chloroplast proteins

Labeling of thylakoid protein was performed as previously described (Armbruster et al. 2010) on young leaf discs from 6-week-(WT) and 10-week-(mutants) old plants (at comparable developmental stage) at 3 h after the start of the photo-period (Supplemental Fig. S6). Briefly, leaf discs with a 0.5 cm diameter were vacuum-infiltrated with 20 μ g/ml cycloheximide in 10 ml of 10 mM Tris, 5 mM MgCl₂, 20 mM KCl, pH 6.8, and 0.1% (v/v) Tween 20 and incubated for 30 min to block cytosolic translation. For pulse labeling, the leaves were infiltrated again with the same solution containing 1 mCi of [³⁵S] methionine and transferred into ambient light ($\sim 10 \mu\text{mol photons m}^{-2} \text{s}^{-1}$) for 20 min. Then, thylakoid isolation and BN-PAGE were performed as described above. Following the pulse labeling, leaves were incubated again with 10 mM of unlabeled methionine for 20 min in light (chase labeling) and processed further as described above. Signals were detected using Storage phosphor screens (Fujifilm) and visualized using the Amersham Typhoon RGB Biomolecular Imager (GE Healthcare Life Sciences).

Accession numbers

DEAP2 sequences from Arabidopsis (At3g51510), *Glycine max* (Glyma.03G158200), *Oryza sativa* (Os05g41190), *Sorghum bicolor* (Sobic.009G179800), *Zea mays* (ZMPHB47.06G250900), *Sphagnum maghellanicum* (Sphmag03G126700) and *Physcomitrium patens* (Pp3ca2_25230), *Volvox carteri* (Vocar.0018 s0093), and *Chlamydomonas reinhardtii* (Cre16.g679300) and PAM68 and LPA1 from Arabidopsis (At4g19100 and At1g02910, respectively).

Acknowledgments

The authors thank Paulina Heinkow for excellent technical assistance within the MS Proteomics Unit Biology of Plants of the University of Münster.

Author contributions

M.J.F. selected T-DNA insertion lines, made complementation lines, and tested the antibody. O.S.I. generated additional mutants by CRISPR-Cas employing expertise from R.B. S.K. generated double mutants. J.M.K. performed most

experiments with the help of L.J. and N.W. J.E. and I.F. performed MS analyses and interpretations. M.A.S. and W.T. quantified complexes and pigments and measured photosynthetic parameters. I.G. and R.Z. performed ribosome profiling. T.R. predicted protein structure. J.M.K., U.A., R.Z., M.A.S., and D.S. interpreted data. U.A. wrote manuscript together with J.M.K. and help from all authors.

Supplemental data

The following materials are available in the online version of this article.

Supplemental Figure S1. Selection of At3g51510 T-DNA insertion lines.

Supplemental Figure S2. CRISPR-Cas deletion lines of DEAP2.

Supplemental Figure S3. Volcano plot analysis of changes in transcript and translation efficiency between *deap2-1* and *pam68-2* compared with WT.

Supplemental Figure S4. Graphical representation of common significant differences in both *deap2-1* and *pam68-2* mutants compared with WT.

Supplemental Figure S5. 2D-BN-PAGE analysis of solubilized *cDEAP2-1* thylakoid complexes.

Supplemental Figure S6. Leaf discs used for in vivo labeling.

Supplemental Figure S7. Double mutant of *pam68* with *deap2* but not with *lpa1* show a lack of functional PSII.

Supplemental Figure S8. Selection and characterization of DEAP2 and PAM68 expressing mutants.

Supplemental Figure S9. Relative quantification of DEAP2 and PAM68.

Supplemental Table S1. Proteins detected by mass spectrometry analysis of DEAP2-specific coimmunoprecipitation experiments.

Supplemental Table S2. Peptides of At3G51510 (DEAP2) found by mass spectrometry analysis as shown in Supplemental Table S1.

Supplemental Table S3. Spectroscopic analysis of photosynthesis-related parameters.

Supplemental Table S4. Ribosome profiling of *deap2-1* and WT.

Supplemental Table S5. Ribosome profiling of *pam68-2* and WT.

Supplemental Table S6. Analysis of transcripts, footprints, and resulting translational efficiencies of *deap2-1* and *pam68-2* compared with WT.

Supplemental Table S7. Summary of the ribosome profiling results.

Supplemental Table S8. Primers used in this study.

Funding

J.M.K., U.A., M.A.S., R.Z., and R.B. received funding from the Max Planck society and R.Z. and I.F. from the Deutsche

Forschungsgemeinschaft (DFG # 437345987 and 445970965, 469950637, respectively).

Data availability

MS raw data were deposited via JPOST (Moriya et al. 2019, <https://repository.jpostdb.org/>).

References

- Alonso JM, Stepanova AN, Leisse TJ, Kim CJ, Chen H, Shinn P, Stevenson DK, Zimmerman J, Barajas P, Cheuk R, et al. Genome-wide insertional mutagenesis of *Arabidopsis thaliana*. *Science*. 2003;301(5633):653–657. <https://doi.org/10.1126/science.1086391>
- Armbruster U, Carrillo LR, Venema K, Pavlovic L, Schmidtman E, Kornfeld A, Jahns P, Berry JA, Kramer DM, Jonikas MC. Ion antiport accelerates photosynthetic acclimation in fluctuating light environments. *Nat Commun*. 2014;5(1):5439. <https://doi.org/10.1038/ncomms6439>
- Armbruster U, Zühlke J, Rengstl B, Kreller R, Makarenko E, Rühle T, Schünemann D, Jahns P, Weisshaar B, Nickelsen J, et al. The *Arabidopsis* thylakoid protein PAM68 is required for efficient D1 biogenesis and photosystem II assembly. *Plant Cell*. 2010;22(10):3439–3460. <https://doi.org/10.1105/tpc.110.077453>
- Armenteros JJA, Salvatore M, Emanuelsson O, Winther O, Heijne GV, Elofsson A, Nielsen H. Detecting sequence signals in targeting peptides using deep learning. *Life Sci Alliance*. 2019;2(5):e201900429. <https://doi.org/10.26508/lsa.201900429>
- Benjamini Y, Hochberg Y. Controlling the false discovery rate: a practical and powerful approach to multiple testing. *J R Stat Soc Series B Methodol*. 1995;57(1):289–300. <https://doi.org/10.1111/j.2517-6161.1995.tb02031.x>
- Blatt MR, Grefen C. Applications of fluorescent marker proteins in plant cell biology. *Methods Mol Biol*. 2014;1062:487–507. https://doi.org/10.1007/978-1-62703-580-4_26
- Bučinská L, Kiss E, Konik P, Knoppova J, Komenda J, Sobotka R. The ribosome-bound protein Pam68 promotes insertion of chlorophyll into the CP47 subunit of photosystem II. *Plant Physiol*. 2018;176(4):2931–2942. <https://doi.org/10.1104/pp.18.00061>
- Clough SJ, Bent AF. Floral dip: a simplified method for *Agrobacterium*-mediated transformation of *Arabidopsis thaliana*. *Plant J*. 1998;16(6):735–743. <https://doi.org/10.1046/j.1365-313x.1998.00343.x>
- Cox J, Mann M. MaxQuant enables high peptide identification rates, individualized p.p.b.-range mass accuracies and proteome-wide protein quantification. *Nat Biotechnol*. 2008;26(12):1367–1372. <https://doi.org/10.1038/nbt.1511>
- Davis IW, Leaver-Fay A, Chen VB, Block JN, Kapral GJ, Wang X, Murray LW, Arendall WB, 3rd, Snoeyink J, Richardson JS, et al. MolProbity: all-atom contacts and structure validation for proteins and nucleic acids. *Nucleic Acids Res*. 2007;35(Web Server):W375–W383 <https://doi.org/10.1093/nar/gkm216>
- Earley KW, Haag JR, Pontes O, Opper K, Juehne T, Song K, Pikaard CS. Gateway-compatible vectors for plant functional genomics and proteomics. *Plant J*. 2006;45(4):616–629. <https://doi.org/10.1111/j.1365-313x.2005.02617.x>
- Fu HY, Ghandour R, Ruf S, Zoschke R, Bock R, Schöttler MA. The availability of neither D2 nor CP43 limits the biogenesis of photosystem II in tobacco. *Plant Physiol*. 2021;185(3):1111–1130. <https://doi.org/10.1093/plphys/kiaa052>
- Gao Y, Thiele W, Saleh O, Scossa F, Arabi F, Zhang H, Sampathkumar A, Kuhn K, Fernie A, Bock R, et al. Chloroplast translational regulation uncovers nonessential photosynthesis genes as key players in plant cold acclimation. *Plant Cell*. 2022;34(5):2056–2079. <https://doi.org/10.1093/plcell/koac056>

- Ghandour R, Gao Y, Laskowski J, Barahimipour R, Ruf S, Bock R, Zoschke R.** Transgene insertion into the plastid genome alters expression of adjacent native chloroplast genes at the transcriptional and translational levels. *Plant Biotechnol J.* 2023;**21**(4):711–725. <https://doi.org/10.1111/pbi.13985>
- Gibson DG, Young L, Chuang RY, Venter JC, Hutchison CA 3rd, Smith HO** (2009) Enzymatic assembly of DNA molecules up to several hundred kilobases. *Nat Methods* **6**(5):343–345 <https://doi.org/10.1038/nmeth.1318>
- Hallgren J, Tsigirgos KD, Pedersen MD, Armenteros JJA, Marcantili P, Nielsen H, Krogh A, Winther O.** DeepTMHMM predicts alpha and beta transmembrane proteins using deep neural networks. *bioRxiv* 2022.2004.2008.487609. 2022, preprint: not peer reviewed.
- Jumper J, Evans R, Pritzel A, Green T, Figurnov M, Ronneberger O, Tunyasuvunakool K, Bates R, Židek A, Potapenko A, et al.** Highly accurate protein structure prediction with AlphaFold. *Nature.* 2021; **596**(7873):583–589. <https://doi.org/10.1038/s41586-021-03819-2>
- Karnauchov I, Herrmann RG, Klösgen RB.** Transmembrane topology of the rieske Fe/S protein of the cytochrome b6/f complex from spinach chloroplasts. *FEBS Lett.* 1997;**408**(2):206–210. [https://doi.org/10.1016/S0014-5793\(97\)00427-4](https://doi.org/10.1016/S0014-5793(97)00427-4)
- Karpowicz SJ, Prochnik SE, Grossman AR, Merchant SS.** The GreenCut2 resource, a phylogenomically derived inventory of proteins specific to the plant lineage *. *J Biol Chem.* 2011;**286**(24):21427–21439. <https://doi.org/10.1074/jbc.M111.233734>
- Kirchhoff H, Mukherjee U, Galla HJ.** Molecular architecture of the thylakoid membrane: lipid diffusion space for plastoquinone. *Biochemistry.* 2002;**41**(15):4872–4882. <https://doi.org/10.1021/bi011650y>
- Komenda J, Reisinger V, Müller BC, Dobáková M, Granvogl B, Eichacker LA.** Accumulation of the D2 protein is a key regulatory step for assembly of the photosystem II reaction center complex in *Synechocystis* PCC 6803*. *J Biol Chem.* 2004;**279**(47):48620–48629. <https://doi.org/10.1074/jbc.M405725200>
- Komenda J, Sobotka R, Nixon PJ.** Assembling and maintaining the photosystem II complex in chloroplasts and cyanobacteria. *Curr Opin Plant Biol.* 2012;**15**(3):245–251. <https://doi.org/10.1016/j.pbi.2012.01.017>
- Kunst L.** Preparation of physiologically active chloroplasts from *Arabidopsis*. In: **Martinez-Zapater JM, Salinas J**, editors. *Arabidopsis protocols*. Totowa, NJ: Humana Press; 1998. p. 43–48.
- Li Y, Liu B, Zhang J, Kong F, Zhang L, Meng H, Li W, Rochaix JD, Li D, Peng L.** OHP1, OHP2, and HCF244 form a transient functional complex with the photosystem II reaction center. *Plant Physiol.* 2019;**179**(1):195–208. <https://doi.org/10.1104/pp.18.01231>
- Li HM, Moore T, Keegstra K.** Targeting of proteins to the outer envelope membrane uses a different pathway than transport into chloroplasts. *Plant Cell.* 1991;**3**(7):709–717. <https://doi.org/10.1105/tpc.3.7.709>
- Link S, Engelmann K, Meierhoff K, Westhoff P.** The atypical short-chain dehydrogenases HCF173 and HCF244 are jointly involved in translational initiation of the psbA mRNA of *Arabidopsis*. *Plant Physiol.* 2012; **160**(4):2202–2218. <https://doi.org/10.1104/pp.112.205104>
- Lu Y.** Identification and roles of photosystem II assembly, stability, and repair factors in *Arabidopsis*. *Front Plant Sci.* 2016;**7**:168. <https://doi.org/10.3389/fpls.2016.00168>
- Meurer J, Plücker H, Kowallik KV, Westhoff P.** A nuclear-encoded protein of prokaryotic origin is essential for the stability of photosystem II in *Arabidopsis thaliana*. *EMBO J.* 1998;**17**(18):5286–5297. <https://doi.org/10.1093/emboj/17.18.5286>
- Moriya Y, Kawano S, Okuda S, Watanabe Y, Matsumoto M, Takami T, Kobayashi D, Yamanouchi Y, Araki N, Yoshizawa AC, et al.** The jPOST environment: an integrated proteomics data repository and database. *Nucleic Acids Res.* 2019;**47**(D1):D1218–D1224. <https://doi.org/10.1093/nar/gky899>
- Myouga F, Takahashi K, Tanaka R, Nagata N, Kiss AZ, Funk C, Nomura Y, Nakagami H, Jansson S, Shinozaki K.** Stable accumulation of photosystem II requires ONE-HELIX PROTEIN1 (OHP1) of the light harvesting-like family. *Plant Physiol.* 2018;**176**(3):2277–2291. <https://doi.org/10.1104/pp.17.01782>
- Nickelsen J, Rengstl B.** Photosystem II assembly: from cyanobacteria to plants. *Annu Rev Plant Biol.* 2013;**64**(1):609–635. <https://doi.org/10.1146/annurev-arplant-050312-120124>
- Peng L, Ma J, Chi W, Guo J, Zhu S, Lu Q, Lu C, Zhang L.** LOW PSII ACCUMULATION1 is involved in efficient assembly of photosystem II in *Arabidopsis thaliana*. *Plant Cell.* 2006;**18**(4):955–969. <https://doi.org/10.1105/tpc.105.037689>
- Peng L, Shimizu H, Shikanai T.** The chloroplast NAD(P)H dehydrogenase complex interacts with photosystem I in *Arabidopsis*. *J Biol Chem.* 2008;**283**(50):34873–34879. <https://doi.org/10.1074/jbc.M803207200>
- Porra RJ, Thompson WA, Kriedemann PE.** Determination of accurate extinction coefficients and simultaneous equations for assaying chlorophylls a and b extracted with four different solvents: verification of the concentration of chlorophyll standards by atomic absorption spectroscopy. *Biochim Biophys Acta Bioenerg.* 1989;**975**(3):384–394. [https://doi.org/10.1016/S0005-2728\(89\)80347-0](https://doi.org/10.1016/S0005-2728(89)80347-0)
- Rokka A, Suorsa M, Saleem A, Battchikova N, Aro EM.** Synthesis and assembly of thylakoid protein complexes: multiple assembly steps of photosystem II. *Biochem J.* 2005;**388**(1):159–168. <https://doi.org/10.1042/BJ20042098>
- Schägger H.** Tricine-SDS-PAGE. *Nat Protoc.* 2006;**1**(1):16–22. <https://doi.org/10.1038/nprot.2006.4>
- Schöttler MA, Flügel C, Thiele W, Stegemann S, Bock R.** The plastome-encoded Psaj subunit is required for efficient photosystem I excitation, but not for plastocyanin oxidation in tobacco. *Biochem J.* 2007;**403**(2):251–260. <https://doi.org/10.1042/BJ20061573>
- Schöttler MA, Kirchhoff H, Weis E.** The role of plastocyanin in the adjustment of the photosynthetic electron transport to the carbon metabolism in tobacco. *Plant Physiol.* 2004;**136**(4):4265–4274. <https://doi.org/10.1104/pp.104.052324>
- Schreiber U, Klughammer C.** Analysis of photosystem I donor and acceptor sides with a new type of online-deconvoluting kinetic LED-array spectrophotometer. *Plant Cell Physiol.* 2016;**57**(7):1454–1467. <https://doi.org/10.1093/pcp/pcw044>
- Schuster M, Gao Y, Schöttler MA, Bock R, Zoschke R.** Limited responsiveness of chloroplast gene expression during acclimation to high light in tobacco. *Plant Physiol.* 2020;**182**(1):424–435. <https://doi.org/10.1104/pp.19.00953>
- Shen JR.** The structure of photosystem II and the mechanism of water oxidation in photosynthesis. *Annu Rev Plant Biol.* 2015;**66**(1):23–48. <https://doi.org/10.1146/annurev-arplant-050312-120129>
- Shevela D, Ananyev G, Vatland AK, Arnold J, Mamedov F, Eichacker LA, Dismukes GC, Messinger J.** ‘Birth defects’ of photosystem II make it highly susceptible to photodamage during chloroplast biogenesis. *Physiol Plant.* 2019;**166**(1):165–180. <https://doi.org/10.1111/ppl.12932>
- Shevela D, Arnold J, Reisinger V, Berends HM, Kmiec K, Koroidov S, Bue AK, Messinger J, Eichacker LA.** Biogenesis of water splitting by photosystem II during de-etiolation of barley (*Hordeum vulgare* L.). *Plant Cell Environ.* 2016;**39**(7):1524–1536. <https://doi.org/10.1111/pce.12719>
- Trösch R, Barahimipour R, Gao Y, Badillo-Corona JA, Gotsmann VL, Zimmer D, Mühlhaus T, Zoschke R, Willmund F.** Commonalities and differences of chloroplast translation in a green alga and land plants. *Nat Plants.* 2018;**4**(8):564–575. <https://doi.org/10.1038/s41477-018-0211-0>
- Wei X, Su X, Cao P, Liu X, Chang W, Li M, Zhang X, Liu Z.** Structure of spinach photosystem II–LHCII supercomplex at 3.2 Å resolution. *Nature.* 2016;**534**(7605):69–74. <https://doi.org/10.1038/nature18020>
- Zagari N, Sandoval-Ibañez O, Sandal N, Su J, Rodriguez-Concepcion M, Stougaard J, Pribil M, Leister D, Pulido P.** SNOWY COTYLEDON 2 promotes chloroplast development and has a role in leaf variegation in both *Lotus japonicus* and *Arabidopsis thaliana*. *Mol Plant.* 2017;**10**(5):721–734. <https://doi.org/10.1016/j.molp.2017.02.009>

Zhou X, Zheng W, Li Y, Pearce R, Zhang C, Bell EW, Zhang G, Zhang Y. I-TASSER-MTD: a deep-learning-based platform for multi-domain protein structure and function prediction. *Nat Protoc.* 2022;**17**(10): 2326–2353. <https://doi.org/10.1038/s41596-022-00728-0>

Zoschke R, Barkan A. Genome-wide analysis of thylakoid-bound ribosomes in maize reveals principles of cotranslational targeting to the thylakoid membrane. *Proc Natl Acad Sci USA* 2015;**112**(13): E1678-1687. <https://doi.org/10.1073/pnas.1424655112>